Available online at www.sciencedirect.com
SCIENCE DIRECT
Journal of Catalysis 239 (2006) 390–401
JOURNAL OF CATALYSIS
www.elsevier.com/locate/jcat

Kinetics and mechanism of cyclohexane oxidation on MnAPO-5 catalysts ☆

Björn Modén [a], Bi-Zeng Zhan [a], Jihad Dakka [b], José G. Santiesteban [b], Enrique Iglesia [a,*]

[a] *Department of Chemical Engineering, University of California at Berkeley, Berkeley, CA 94720, USA*
[b] *Corporate Strategic Research, ExxonMobil Research and Engineering Co., Route 22 East, Annandale, NJ 08801, USA*

Received 30 November 2005; revised 17 January 2006; accepted 10 February 2006

Available online 20 March 2006

Abstract

Kinetic and isotopic measurements have led to a detailed description of the elementary steps required for cyclohexane (RH) reactions with O_2 on MnAPO-5 catalysts. Cyclohexyl hydroperoxide (ROOH) is an intermediate in cyclohexanol (ROH) and cyclohexanone [R(–H)=O] formation. Combined rates of ROH + R(–H)=O synthesis are first order in ROOH concentration and proportional to the number of redox-active framework Mn sites. Taken together with UV–visible evidence for Mn^{2+} as the most abundant active structure during steady-state catalysis, these data indicate that ROOH decomposition on Mn^{2+} is a kinetically relevant step. C_6H_{12}/C_6D_{12} kinetic isotope effects (KIE) for ROOH decomposition as a function of ROOH concentration are 2.5 at 403 K, consistent with O–H bond cleavage at Mn^{2+}–O–H in this elementary step. A catalytic ROOH decomposition cycle proceeding via adsorbed intermediates without the involvement of free radicals or their bimolecular termination accounts for measured alcohol/ketone product ratios. Mn^{3+} species, initially present in air-treated MnAPO-5, activate R–H bonds and lead to shorter initial induction periods for ROOH-mediated pathways. *tert*-Butyl hydroperoxide (TBHP) led to higher ROOH synthesis rates via H abstraction from RH to form ROOH, without influencing ROOH decomposition rate constants. In the absence of TBHP, ROOH formation occurs predominantly through activation of C–H bonds in RH by ROO* species in a step that gives a KIE value of 6.8, consistent with such activation steps. These findings are expected to be also relevant for related RH oxidation reactions on materials containing redox-active sites such as inorganic solids or solvated cations. The proposed sequence of elementary steps illustrates the difficulties in interpreting effects of isotopic identity on rates and of spatial constraints on regioselectivity without rigorous assessment of the identity and kinetic relevance of elementary steps, and also the risk of using overall KIE values as phenomenological inference for a certain mechanism, particularly for sequential pathways, such as the ROOH formation and ROOH decomposition steps discussed here.

Keywords: Cyclohexane oxidation; MnAPO-5; Kinetics; Isotope effects

1. Introduction

Selective oxidation of alkanes to valuable oxygen-containing molecules remains a formidable challenge [1–3], because desired products sequentially convert to CO_x and the position of oxygen attachment is dictated solely by C–H bond energies [4,5]. Aluminophosphate molecular sieves (AlPO-n) are microporous crystalline materials [6,7] that can accommodate framework substitutions by transition metal cations to give MeAPO-n materials (Me = metal) [8–10]. These materials combine the reactivity of redox-active cations (e.g., Co, Mn, and Fe) with the unique spatial constraints provided by small channels (3.5–12 Å). MeAPO materials catalyze alkane oxidation to alcohols, aldehydes, ketones, and acids using O_2 or *tert*-butyl hydroperoxide (TBHP) as oxidants [11–26]. Small channels in CoAPO-18 and MnAPO-18 have been claimed to promote selective oxygen attachment at terminal carbon atoms via collimation of *n*-alkanes and to direct activation toward terminal C–H bonds on active oxygen species at metal framework sites [18–21]; to the best of our knowledge, these unusual selectivities have remained unconfirmed by later studies.

☆ This manuscript is dedicated to Dr. Heinz Heinemann, a colleague and friend, and a pioneer and role model in the development of modern heterogeneous catalysis. Dr. Heinemann passed away on November 23, 2005 as we were completing the final draft of this manuscript.

* Corresponding author. Fax: +1 510 642 4778.
E-mail address: iglesia@berkeley.edu (E. Iglesia).

0021-9517/$ – see front matter
doi:10.1016/j.jcat.2006.02.006

The details of the mechanism of alkane oxidation remain unclear [3]; yet these details are essential for the control and definitive elucidation of any effects of spatial constraints on rates and selectivities. Framework cations are thought to act as redox centers that form radical-like intermediates, in analogy with oxidation pathways on solvated cations in liquid media [1,2], but independent kinetic or isotopic evidence is not available. In these mechanistic proposals, redox centers decompose alkyl hydroperoxide (ROOH) intermediates via Haber–Weiss radical mechanisms, but do not activate C–H bonds in alkanes via direct reactions with O_2 [1,2,27,28]. Me–OOR (Me = Co, Mn, Fe; R = alkyl) complexes, proposed as intermediates in ROOH decomposition, have been synthesized; their decomposition rates are consistent with their proposed role in alkane–O_2 reactions [29,30].

Cyclohexane oxidation rates on MnAPO-5 catalysts are proportional to the number of redox-active Mn centers (Mn_{redox}), measured by H_2–O_2 reduction–oxidation cycles, indicating that these species act as active sites for kinetically relevant elementary steps in alkane oxidation catalytic cycles [31]. Here we explore the nature of these rate-limiting steps and propose a set of elementary steps consistent with all available kinetic and isotopic data and with sequential oxidation pathways involving ROOH intermediates. In a separate report [32], we discuss reactant and transition-state oxidation shape selectivity on MeAPO materials in the context of these elementary steps.

2. Experimental

2.1. Synthesis and characterization of MnAPO-5 samples

MnAPO-5 samples were prepared as described previously [7]. Mn was introduced during synthesis as divalent cations to give materials with Mn/P atomic ratios of 0.028–0.10. X-ray diffraction patterns for all samples showed the expected AlPO-5 pattern, and no other crystalline phases were detected. The crystallite sizes determined by scanning electron microscopy were 5–10 μm. Samples were treated in flowing dry air (8.33 $cm^3\,s^{-1}\,g^{-1}$; Airgas, zero grade; purified with a 13X sieve held at ambient temperature) by heating to 393 K at 0.167 $K\,s^{-1}$, holding for 1 h, and then heating to 773 K at 0.05 $K\,s^{-1}$ and holding for 3 h. Chemical compositions were determined by inductively coupled plasma emission spectroscopy (Table 1). The fraction of the Mn atoms present as redox-active cations (Mn_{redox}/Mn_{total}) was measured from the amount of H_2 consumed during thermal treatment in H_2 [31]. The Mn oxidation state was determined before and after catalytic reactions by diffuse reflectance UV–visible spectroscopy using a Cary 400 Varian spectrophotometer [31].

Table 1
Elemental composition and redox-active fraction[a] for MnAPO-5 materials

Catalyst	Atomic fractions		Mn_{redox} fraction[a]
	Mn/P	Al/P	Mn_{redox}/Mn_{total}
MnAPO-5(0.028)	0.028	0.972	0.70
MnAPO-5(0.055)	0.055	0.982	0.62
MnAPO-5(0.10)	0.100	0.945	0.40

[a] From Ref. [31].

2.2. Cyclohexane oxidation reactions on MnAPO-5

Catalytic oxidation rates and selectivities were measured for cyclohexane substrates (25 cm^3; Aldrich, 99.99%) in a shielded high-pressure glass reactor (Andrews Glass; 100 cm^3) using 0.2 g of catalyst, transferred into the reactor after treating the samples in dry air (as described above) without intervening exposure to ambient air. The reactor pressure was increased to ∼0.4 MPa using pure O_2 (Airgas, UHP) at ambient temperature before heating rapidly to 403 K, which led to a final pressure of 0.7 MPa (0.55 MPa O_2 and 0.15 MPa cyclohexane vapor pressure) at 403 K. O_2 was added during the reaction to maintain the total pressure at 0.70 ± 0.01 MPa. Reaction rates and selectivities were measured at 388, 403, and 413 K. Liquid samples (∼0.5 cm^3) were extracted periodically, and the concentrations of reactants and products were measured by gas chromatography (Agilent 5890; DB-wax column: 60 m long, 0.32 mm i.d., 0.5 μm film thickness) using a flame ionization detector and *o*-dichlorobenzene (0.2 cm^3) as an internal standard. Cyclohexanol, cyclohexanone, and cyclohexyl hydroperoxide were the most abundant products, but acids (e.g., adipic acid) were also detected (at <5% selectivity), especially at high conversions (>3%). Cyclohexyl hydroperoxide concentrations were measured after reaction with triphenylphosphine (Sigma–Aldrich) to form cyclohexanol [33]. Differential rates were measured by fitting ROH, R(–H)=O, and ROOH concentration time data (typically 8–15 data points) with a fourth-order polynomial to determine local derivatives with respect to time.

Framework cations can leach into liquid reaction media [34,35] and cause structural degradation and the appearance of catalysis by solvated cations. For instance, Co cations leach from CoAPO materials during cyclohexane oxidation in acetic acid, but not with alkanes as solvents [16]. Any leaching of Mn species and its consequent contributions to ROOH decomposition pathways on solvated Mn cations were probed by carrying out cyclohexane oxidation with MnAPO-5 and then continuing the reaction with the decanted liquid free of solids. The reaction was carried out for 4 h (to ∼1% conversion); the catalyst was allowed to settle for 180 s and the hot liquid was decanted into an empty reactor, within which the reaction was continued without adding catalyst.

tert-Butyl hydroperoxide (TBHP; 70% in H_2O, Sigma–Aldrich) was used in some experiments (10 TBHP/Mn_{redox}; ∼0.1 mL TBHP/H_2O in 25 cm^3 cyclohexane) to initiate autoxidation reactions while maintaining O_2 as the predominant stoichiometric oxidant. These experiments were carried out for at least 100 turnovers (per Mn_{redox}); the stoichiometric use of TBHP would have sufficed for only ∼10 turnovers.

Kinetic isotope effect (KIEs) and isotopic tracer measurements were performed using C_6H_{12} and C_6D_{12} (Cambridge Isotope Labs, 99.6% isotopic purity) either separately or as equimolar C_6H_{12}–C_6D_{12} mixtures. Reactant and product concentrations were measured as described above and also by mass spectrometry (Agilent 5973) after chromatographic separation

(Agilent 6890) using either a DB-wax column (60 m long, 0.32 mm i.d., and 0.5 μm film thickness) or a methyl-silicone HP-1 column (50 m long, 0.32 mm i.d., and 0.5 μm film thickness).

3. Results and discussion

3.1. Cyclohexane oxidation reaction pathways and elementary steps on MnAPO-5

The conversions of cyclohexane (RH) to cyclohexanol (ROH), cyclohexanone (R(–H)=O), and cyclohexyl hydroperoxide (ROOH) are shown in Fig. 1 as a function of time on MnAPO-5 (Mn/P = 0.055, pretreated in dry air at 773 K) at 403 K. ROOH is the predominant product during an initial induction period (∼0.5 h) before R(–H)=O and ROH become detectable. The cyclohexyl hydroperoxide selectivity was initially ∼100% and decreased with contact time, consistent with its involvement as a reactive intermediate in the formation of R(–H)=O and ROH, as proposed for solvated Co and Mn catalysts in homogeneous media [1,28].

The effects of ROOH concentration on cyclohexane oxidation turnover rates were measured from the combined rates of formation of ROH and R(–H)=O as ROOH concentration increased with increasing contact time (Fig. 2). In all cases, product formation rates were proportional to [ROOH], consistent with its kinetic relevance as a reactive intermediate in ROH and R(–H)=O formation. First-order rate constants per Mn_{redox} were similar (0.37–0.46 h^{-1} Mn_{redox}^{-1} [ROOH, mM]$^{-1}$) on MnAPO-5 catalysts with Mn/P ratios of 0.028–0.10, indicating that kinetically relevant ROOH decomposition steps are catalyzed by redox-active Mn-sites, not by permanently divalent sites also present in these samples, and do not occur via homogeneous autoxidation pathways (Table 2) [31]. These similar rate constants indicate that the rates are kinetic in nature and unaffected by transport restrictions, which would have restricted more severely measured rates more severely on samples with higher active site concentrations.

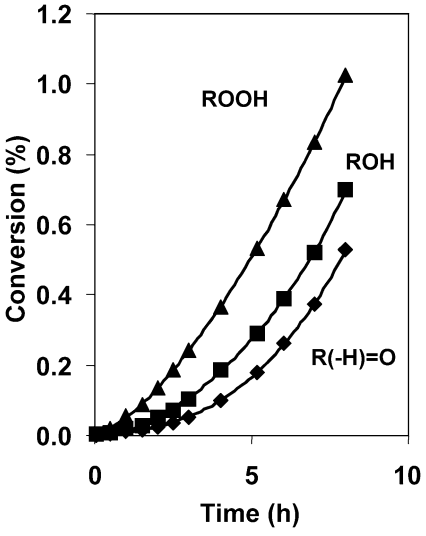

Fig. 1. Conversion (%) to cyclohexanol (ROH, ■), cyclohexanone (R(–H)=O, ◆), and cyclohexyl hydroperoxide (ROOH, ▲) [403 K, 25 mL cyclohexane, 0.55 MPa O_2, 0.2 g MnAPO-5(0.055)].

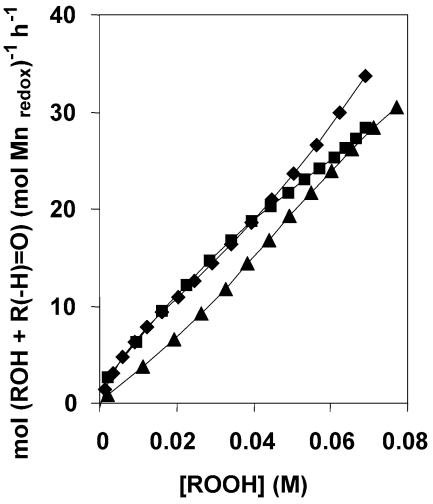

Fig. 2. Effect of ROOH concentration on cyclohexane turnover rates per Mn_{redox} for MnAPO-5 with Mn/P ratios of 0.028 (▲), 0.055 (◆) and 0.10 (■) [403 K, 25 mL cyclohexane, 0.55 MPa O_2, 0.2 g catalyst].

Table 2
Cyclohexanol + cyclohexanone formation rate constants normalized by Mn_{redox} or $Mn_{non\text{-}redox}$ and [ROOH] [403 K, 25.0 mL cyclohexane, 0.55 MPa O_2, 0.20 g catalyst]

Catalyst	Mn_{redox} fraction[a]	ROOH decomposition rate constant[b]	
	Mn_{redox}/Mn_{total}	Per Mn_{redox}	Per $Mn_{non\text{-}redox}$
MnAPO-5(0.028)	0.70	0.41	1.01
MnAPO-5(0.055)	0.62	0.46	0.74
MnAPO-5(0.10)	0.40	0.37	0.28

[a] From Ref. [31].
[b] Rate constant of ROOH decomposition per h and per mM ROOH and either per Mn_{redox} or per $Mn_{non\text{-}redox}$.

The UV–visible spectra of MnAPO-5 samples treated in dry air at 773 K (Fig. 3) showed d–d transitions at 12,000–25,000 cm^{-1} typical of Mn^{3+} centers in MnAPO-5 [31]. MnAPO-5 samples are white during cyclohexane oxidation and lack d–d transitions characteristic of Mn^{3+} centers (Fig. 3). Thus, trivalent Mn_{redox} sites initially present in air-treated samples reduce, remain predominantly divalent, and represent the most abundant reactive Mn structure during steady-state oxidation catalysis. Taken together with the first-order kinetic dependence on ROOH concentration, these results indicate that the reaction of ROOH with Mn^{2+} is a kinetically relevant step [step (1) in Scheme 1 below] in cycloalkane oxidation and that Mn^{2+} is the prevalent state of active Mn cations during catalysis.

The role of the initial Mn oxidation state on rates was determined by treating MnAPO-5(0.055) in 1% H_2/Ar at 773 K for 0.5 h, to convert all Mn^{3+} species to Mn^{2+} [31], before catalytic testing. These samples led to lower initial ROOH formation rates than found on samples treated in dry air at 773 K for 3 h before reaction. These data indicate that required initial elementary steps leading to ROOH formation during the induction period are faster on Mn^{3+} than on Mn^{2+} (Fig. 4). First-

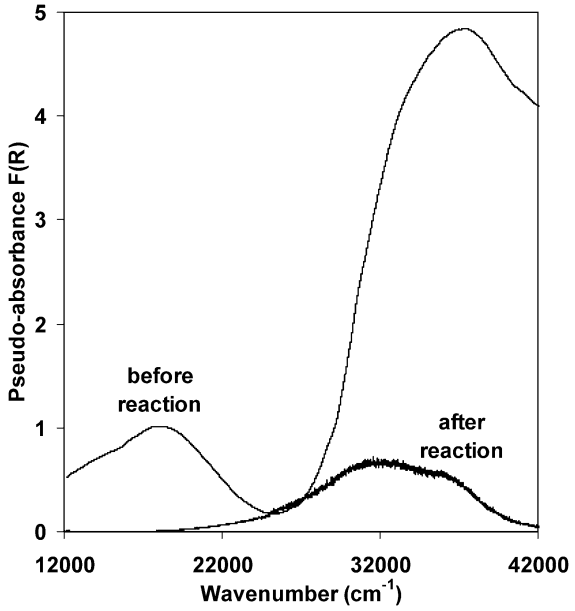

Fig. 3. UV–visible spectra at 298 K of MnAPO-5(0.055) before and after cyclohexane oxidation. Before catalytic experiments the sample was treated in dry air (0.167 K/s to 393 K, 0.05 K/s to 773 K, hold 3 h at 773 K).

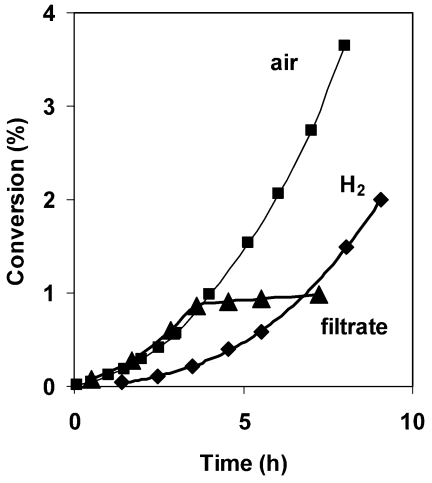

Fig. 4. Total cyclohexane conversion during cyclohexane oxidation on MnAPO-5(0.055) using three different conditions: (i) treated in dry air at 773 K (■), (ii) treated in dry air at 773 K, filtrate removed from reactor at 4 h (▲), (iii) treated in 1% H_2/Ar at 773 K (◆) [403 K, 25 mL cyclohexane, 0.55 MPa O_2, 0.2 g MnAPO-5(0.055)].

order ROOH decomposition rate constants were not influenced by catalyst pretreatment, however, and samples treated in O_2 or H_2 gave identical UV–vis spectra after reaction. ROOH decomposition rates were negligible in the hot decanted liquid collected during leaching tests (Fig. 4), indicating that ROOH decomposition occurred exclusively on framework cations within MnAPO-5 during cyclohexane reactions. Any leaching of active species into the liquid phase did not contribute to measured oxidation rates.

Previous studies have suggested that Me^{n+}[ROOH] complexes ($n = 2$ or 3) form during alkane oxidation on solvated Co and Mn cations and decompose to form alkoxy (RO) and alkylperoxy (ROO) free radicals that propagate and ultimately

$$H^* + ROOH \rightarrow RO^* + H_2O, \quad (1)$$

$$RO^* + R'H \rightarrow R'^* + ROH, \quad (2)$$

$$R'^* + O_2 \rightarrow R'OO^*, \quad (3)$$

$$R'OO^* \rightarrow OH^* + R'(-H)=O, \quad (4)$$

$$OH^* + RH \rightarrow H^* + ROH, \quad (5)$$

$$R'OO^* + R'H \rightarrow R'^* + R'OOH. \quad (6)$$

Scheme 1. Proposed elementary steps for cyclohexane (RH) oxidation. A schematic cyclic representation of this scheme is shown in Fig. 5, where the structures of H^*, RO^*, R'^*, $R'OO^*$, and OH^* are shown in more detail. The R and R′ notations are used to distinguish different cyclohexyl groups in the bimolecular steps (1)–(6).

terminate in bimolecular steps involving two ROO radicals to form ROH and R(–H)=O oxidation products [28]. This conclusion was reached in an attempt to explain ROH/R(–H)=O ratios (∼2) measured in noncatalytic arylalkane oxidation [36]. Such free-radical pathways appear unnecessary for homogeneous or heterogeneous catalysts, in which transition metal cations or other surface species can retain radical-like intermediates at sites in which they form and catalyze their subsequent transformations to form stable molecules. Thus, it seems prudent to consider alternate pathways consistent with this product stoichiometry, but without contrived bimolecular terminal pathways of free-radical intermediates. The proposed Haber–Weiss radical mechanisms can be translated to a mechanism involving bound intermediates, except for the bimolecular termination step, which would require the reaction between adjacent sites each containing bound ROO species. Such site requirements would be inconsistent with the observed single-site nature of the redox-active Mn sites in these materials [31]. We propose here an alternate set of elementary steps that avoids free-radical intermediates and instead includes bound radical-like species that form ROH and R(–H)=O in a stepwise fashion, leading to initial ROH/R(–H)=O ratios of 2 (Scheme 1).

The stoichiometry of the ROOH decomposition cycle [steps (1)–(5)] is given by

$$ROOH + 2RH + O_2 \rightarrow 2ROH + R(-H)=O + H_2O, \quad (7)$$

which accounts for the measured ROH/R(–H)=O ratios of 2 previously ascribed to ROO recombination steps. ROOH formation from steps (3) and (6) is given by

$$RH + O_2 \rightarrow ROOH. \quad (8)$$

At low conversions, ROH/R(–H)=O ratios are similar to those expected from reaction (7), with initial values slightly above 2 being attributed to ROH formation on trivalent Mn in the process of reaching steady-state rates on divalent Mn. On all samples, measured ROH/R(–H)=O ratios decreased with reaction time, because secondary oxidative dehydrogenation reactions converted ROH to R(–H)=O during RH oxidation (Fig. 6). Such ROH dehydrogenation can occur via steps analogous to those that bring RH molecules into the catalytic cycle; ROH activation is likely to occur more rapidly than RH activation because of the weaker C–H bonds in ROH (386.7 kJ/mol for the α-C–H bond in cyclohexanol; 416.2 kJ/mol for C–H

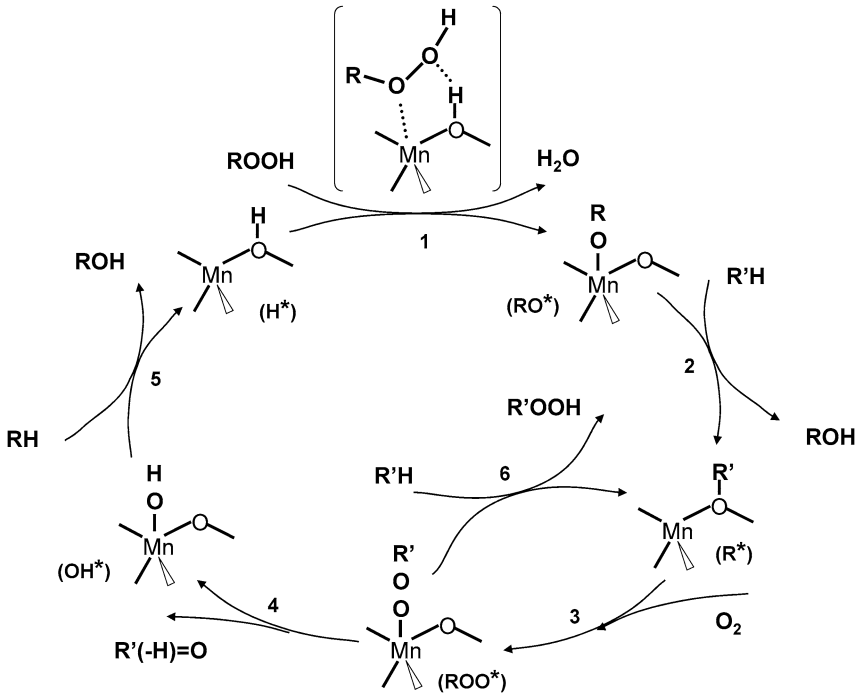

Fig. 5. Catalytic cycle of cyclohexane oxidation on MnAPO-5 catalysts (adapted from Scheme 1).

bonds in cyclohexane [37]). For example, ROH can react with OH^*,

$$OH^* + ROH \rightarrow H^* + R(–H)=O + H_2O, \quad (9)$$

to give R(–H)=O, in a reaction that would lead to a decrease in ROH/R(–H)=O ratios with increasing reaction time. This secondary conversion of ROH to R(–H)=O led us to use combined rates of formation of ROH and R(–H)=O to describe ROOH decomposition rates in our kinetic analysis. The ROOH decomposition cycle [steps (1)–(5) in Fig. 5] gives three ROH + R(–H)=O molecules each time that step (1) occurs [ROOH decomposition; see Eq. (A.7) in Appendix A], leading to an overall ROH and R(–H)=O formation rate of

$$r_{ROH+R(–H)=O} = k_{exp}[ROOH][L] = 3k_1[ROOH][L], \quad (10)$$

in which k_{exp} represents the measured rate constant for ROOH decomposition (the slope in Fig. 2), k_1 is the rate constant for step (1), and [L] is the total number of redox-active sites, corresponding to the number of divalent [H^*] species present as the most abundant surface intermediate (MASI) during cyclohexane oxidation on these catalysts.

We next discuss ROOH formation pathways and the role of radical initiators in ROOH formation and decomposition during cyclohexane (RH) oxidation. The addition of *tert*-butyl hydroperoxide (TBHP, ^{t}BuOOH) led to a marked increase in cyclohexane oxidation rates, predominantly because ROOH species formed more rapidly (Fig. 7a). ROOH decomposition rate constants remained unchanged (Fig. 7b). Thus, TBHP-derived species, such as adsorbed ^{t}BuOO* intermediates, increased only cyclohexyl hydroperoxide formation rates by abstracting hydrogen from cyclohexane in such steps as

$$^tBuOO^* + RH \rightarrow R^* + {}^tBuOOH, \quad (11)$$

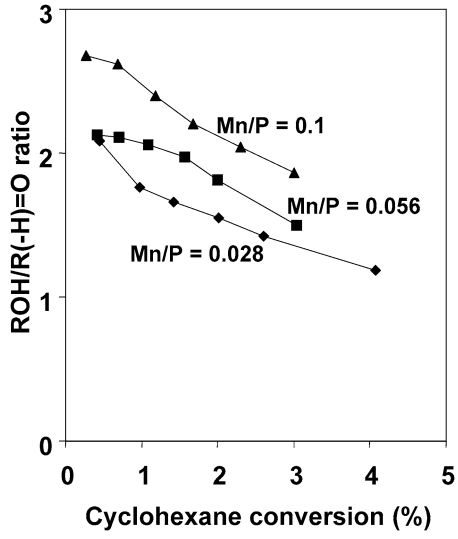

Fig. 6. Alcohol/ketone rate ratio during cyclohexane oxidation for MnAPO-5 with Mn/P ratios of 0.028, 0.055 and 0.10 [403 K, 25 mL cyclohexane, 0.55 MPa O_2, 0.2 g catalyst].

which are then followed by steps (3) and (6) in Scheme 1 to form ROOH. These steps do not influence the rates of ROOH decomposition on redox-active sites.

Fig. 8 shows RH oxidation rates (without TBHP) on MnAPO-5(0.055) pretreated in dry air to oxidize redox-active Mn centers to Mn^{3+} as a function of ROOH concentration. In contrast with ROOH decomposition rates, ROOH formation rates gave a nonzero intercept at low ROOH concentrations and reaction times. This reflects the direct abstraction of H from C–H bonds by Mn^{3+} cations initially present in air-treated samples [Eq. (12)]. In contrast, ROOH formation rates on MnAPO-5 samples treated in 1% H_2/Ar at 773 K for

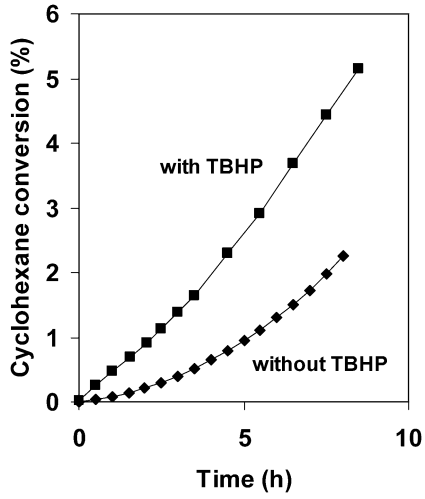

(a)

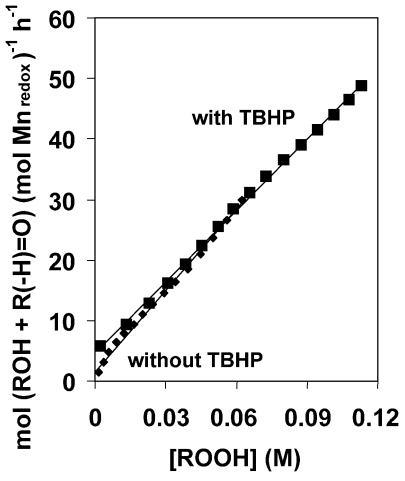

(b)

Fig. 7. (a) Total conversion to cyclohexanol (ROH) + cyclohexanone (R(–H)=O) + cyclohexyl hydroperoxide (ROOH) in the presence (■) and absence (◆) of TBHP initiator. (b) ROH + R(–H)=O formation rates normalized by Mn_{redox} [403 K, 25.0 mL cyclohexane, 0.55 MPa O_2, 0.20 g MnAPO-5(0.055), 10 TBHP/Mn_{redox}].

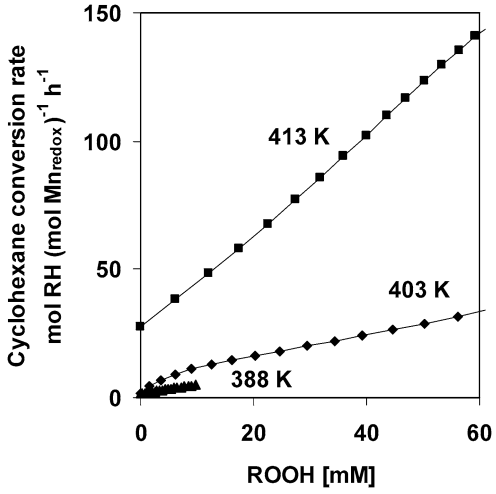

Fig. 8. Cyclohexanol (ROH) + cyclohexanone (R(–H)=O) + cyclohexyl hydroperoxide (ROOH) formation rates vs. [ROOH] for MnAPO-5(0.055) at 388, 403 and 413 K [25 mL cyclohexane, 0.55 MPa O_2, 0.2 g catalyst].

0.5 h before reaction, a process shown to convert all Mn^{3+} to Mn^{2+} [31], gave a zero intercept at low ROOH concentrations, indicating that direct C–H activation, required for the initial formation of ROOH, is much slower on Mn^{2+} than on Mn^{3+} and that ROOH concentrations must build up via homogeneous pathways (Scheme 1) in the absence of Mn^{3+} cations in the starting catalyst.

Air-treated catalysts initially contain predominantly Mn^{3+} sites (*), whereas working catalysts contain only Mn^{2+} sites (H^*). Here we propose a set of reaction steps that account for this reduction process during the initial stages of reaction. All reactants and products in Scheme 1 contain an even number of H atoms, whereas bound intermediates have an odd number; this transition requires that radical-type species with an odd number of H atoms migrate from a site with an even number of H atoms. Initially, RH can react with * through

$$^* + RH \rightarrow R^*H \quad (12)$$

to activate the first C–H bond, followed by O_2 insertion,

$$R^*H + O_2 \rightarrow ROO^*H, \quad (13)$$

to give ROO^*H. ROO^*H can desorb as ROOH,

$$ROO^*H \rightarrow {}^* + ROOH, \quad (14)$$

returning the initial state of the site (*) and providing a sequence of reactions [steps (12)–(14)] that accounts for the role of Mn^{3+} species in the initiation of cyclohexane oxidation and related alkane oxidation reactions. In an alternate step, H or ROO can migrate from ROO^*H to a neighboring * site,

$$ROO^*H + {}^* \rightarrow H^* + ROO^*, \quad (15)$$

leading to two adsorbed species with an odd number of H atoms, which can now enter the catalytic cycle in Scheme 1 via step (1) (H^*) or steps (4) and (6) (ROO^*). Step (15) would have to occur only once for each active site and thus at rates much slower than the catalytic turnovers given by the cycle in Scheme 1.

Activation energies for ROOH decomposition were measured from Arrhenius plots of its rate constant (Fig. 9; 105 ± 10 kJ/mol). Activation energies measured for the initial ROOH formation rates (from the intercepts in Fig. 8 at various temperatures) are significantly higher (155 ± 10 kJ/mol) than those for ROOH decomposition. But these initiation steps must occur only until ROOH concentrations reach levels that allow ROOH formation via more facile pathways involving adsorbed ROO intermediates [e.g., step (6)]. Thus, activation energies for ROOH formation are smaller when ROOH is present, and the initial direct activation of RH by Mn^{3+} [step (12)] is replaced by a sequence of more rapid ROOH formation steps with lower activation energy [e.g., steps (4) and (6)]. These elementary steps involved in ROOH formation and decomposition are discussed below in the context of isotopic studies of cyclohexane oxidation reactions on MnAPO-5. We expect that the conclusions reached here, and confirmed by the isotopic measurements described below, will hold in general for alkane oxidation reactions on materials containing redox-active sites, either as inorganic heterogeneous structures or solvated cations.

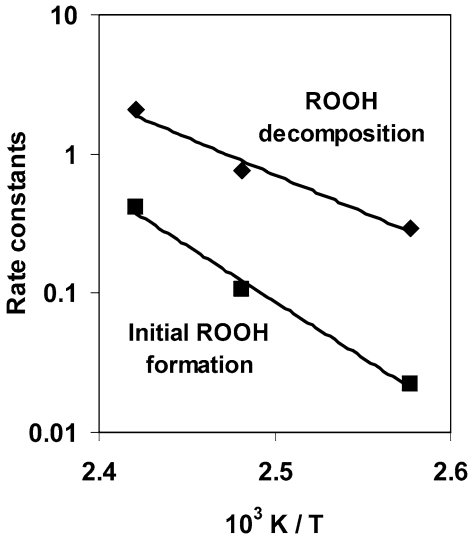

Fig. 9. Arrhenius plot of first order rate constants of ROOH decomposition (◆) and initial ROOH formation (■) per Mn_{redox} and per h [25 mL cyclohexane, 0.55 MPa O_2, 0.2 g MnAPO-5(0.055)].

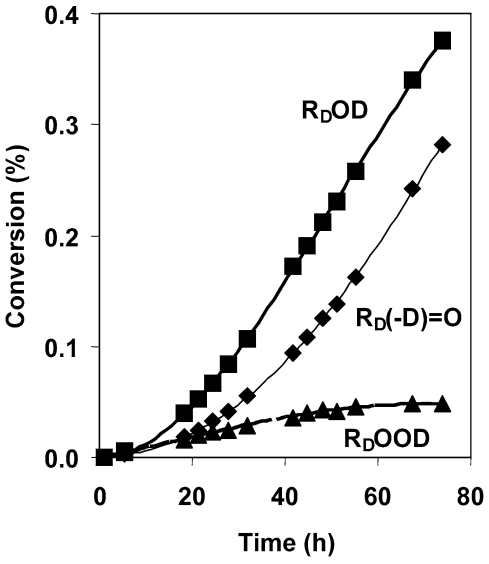

Fig. 10. Conversion (%) of C_6D_{12} to R_DOD (■), $R_D(–D)=O$ (◆), and R_DOOD (▲) [403 K, 25 mL C_6D_{12}, 0.55 MPa O_2, 0.2 g MnAPO-5(0.055)].

3.2. KIEs and isotopic exchange rates

Kinetically relevant elementary steps in cyclohexane oxidation were probed by measuring the effects of replacing H by D in cyclohexane on cyclohexyl hydroperoxide formation and decomposition rates. The conversion of C_6D_{12} (R_DD) to each product [R_DOD, $R_D(–D)=O$, R_DOOD] during C_6D_{12}–O_2 reactions is shown in Fig. 10. At a given reaction time, C_6D_{12} consumption rates were ∼60 times smaller than for C_6H_{12} (Fig. 1). Early transition states for elementary C–H bond activation steps would give KIE values of ∼1 and late transition states, in which the relevant C–H bond is significantly cleaved, give KIE values as high as ∼7 (in the absence of tunneling effects) [38,39]. Thus, measured KIE values (∼60) are much larger than expected for a single elementary step. The sequential nature of cyclohexane oxidation and the large differences in hydroperoxide concentrations between these two reactants combine to give these large apparent KIE values. Below we compare individual rates for the formation and decomposition of R_HOOH and R_DOOD as functions of their respective concentrations.

KIEs for ROOH decomposition were measured from R_HOOH and R_DOOD decomposition rates as a function of [R_HOOH] and [R_DOOD], respectively, in separate C_6H_{12} and C_6D_{12} oxidation experiments. R_HOOH and R_DOOD decomposition rates compared in the region where [R_HOOH] and [R_DOOD] overlap gave a KIE value of 2.5 ± 0.5 for step (1) (denoted as KIE_1) in Scheme 1 (Fig. 11a), typical for primary KIEs [38]. This KIE reflects the cleavage of O–H bonds in the [Me^{2+}–O–H] site by ROOH in step (1) of Scheme 1.

Interpreting KIEs for RH activation is somewhat more difficult, because RH enters the catalytic cycles via steps (2), (5), and (6) in Scheme 1 and also during initial reactions on Mn^{3+} [step (12)]. It is, however, possible to estimate KIE values for some of these steps from measurements of the net and total ROOH and ROH formation rates in separate and mixed C_6H_{12} and C_6D_{12} oxidation experiments. Total product formation rates from C_6H_{12} and C_6D_{12} reactants gave a KIE of 6.0 ± 1.0 for cyclohexane oxidation in the region where [R_HOOH] and [R_DOOD] concentrations overlapped in these experiments (Fig. 11b), whereas the KIEs from equimolar C_6H_{12}–C_6D_{12} mixtures were 5.2 ± 1.0 (Fig. 11c). These KIE values resemble those measured for noncatalytic autoxidation of arylalkanes, in which RO and ROO radicals abstract H atoms from alkyl C–H bonds with a KIE of 5.5 at 333 K [36].

KIEs measured from mixed C_6H_{12}-C_6D_{12} reactants give a more accurate indication of the role of C–H bond activation steps, because C–H and C–D bonds are activated by the same pool of abstracting species throughout the experiment. In contrast, separate C_6H_{12} and C_6D_{12} reactions have very different total [ROOH] concentration ranges, allowing ROOH-based comparisons only within the limited range of [R_DOOD] concentration prevalent for C_6D_{12} reactants. Later, we analyze mixed isotopic data to extract independent KIE values for steps involving RH activation, such as the direct RH oxidation to ROH in step (5) and the RH activation in step (6), the latter of which is the primary route for ROOH formation. This analysis requires that we first measure the extent of isotopic scrambling between C_6H_{12} and C_6D_{12} reactants in mixed experiments, because of its potential effects on the isotopic composition of reactants. We also need to expand the ROOH decomposition kinetic model to account for the presence of intermediates derived from both C_6H_{12} and C_6D_{12}.

We measured the extent of isotopic exchange in mixed C_6H_{12} and C_6D_{12} reactants on MnAPO-5(0.055) at 403 K. Small amounts of C_6D_{12} were converted to $C_6D_{11}H$ (0.08%) after 10 h reaction time; the overall chemical conversion of C_6D_{12} to oxidation products was 0.25%, indicating that exchange rates were ∼30% of chemical conversion rates. Exchange between adsorbed R-groups and alkanes can occur via

$$R_H–H + R_D^* \rightarrow R_H^* + R_D–H, \quad (16)$$

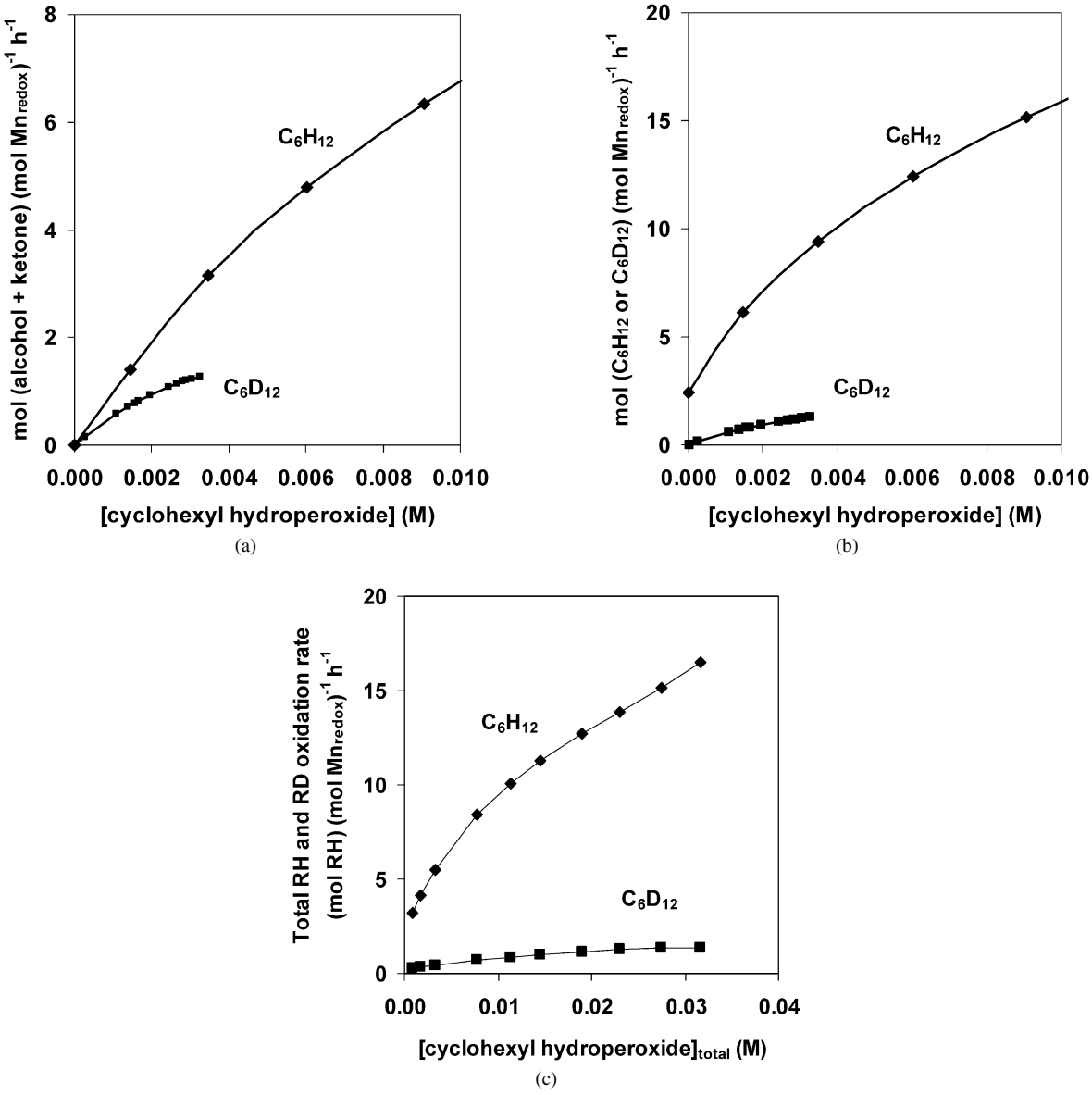

Fig. 11. (a) Interpolated R_HOOH and R_DOOD decomposition rates per Mn_{redox} vs. [R_HOOH] and [R_DOOD] for C_6H_{12} (◆) and C_6D_{12} (■) oxidation on MnAPO-5(0.055). (b) Interpolated C_6H_{12} and C_6D_{12} oxidation rates vs. [R_HOOH] and [R_DOOD] [403 K, 0.55 MPa O_2, 0.2 g MnAPO-5(0.055), 25 mL C_6H_{12} or C_6D_{12}]. (c) C_6H_{12} and C_6D_{12} oxidation rates vs. [$ROOH_{total}$] during mixed C_6H_{12} and C_6D_{12} oxidation [403 K, 0.55 MPa O_2, 0.2 g MnAPO-5(0.055), 25 mL $C_6H_{12} + C_6D_{12}$ (1:1 molar ratio)].

but R_D^* and R_H^* react rapidly with O_2 to generate ROO^* in step (3) of Scheme 1. KIEs for C–H relative to C–D bond activation were ∼6 in these experiments; thus, the incorporation of one H into C_6D_{12} to form $C_6D_{11}H$ and the subsequent activation of the C–H bond in $C_6D_{11}H$ would lead to 1.4 times greater reactivity for $C_6D_{11}H$ relative to C_6D_{12}. The conversion to $C_6D_{11}H$, however, was only 0.08%; thus, overall rates of C_6D_{12} oxidation increased by only a factor of 1.0011 as a result of isotopic scrambling. As a result, the measured extent of isotopic scrambling did not corrupt KIEs for either ROOH formation and decomposition from mixed C_6H_{12}–C_6D_{12} reactants.

With mixed C_6H_{12}–C_6D_{12} reactants, ROOH decomposition occurs on a surface containing an isotopic mixture of H^* and D^* (MASI), instead of only H^* as in the case of C_6H_{12} oxidation. The site balance then becomes

$$[L] = [H^*] + [D^*], \tag{17}$$

because Mn^{2+} is the most abundant surface species during steady-state catalysis. R_H- and R_D-based hydroperoxides (R_HOOH and R_DOOD with O–H and O–D groups) both react with H* and D* to give a total ROOH decomposition rate,

$$r_{ROOH,total} = k_{1,H}[H^*]\big([R_HOOH] + [R_DOOD]\big) + k_{1,D}[D^*]\big([R_HOOH] + [R_DOOD]\big). \tag{18}$$

In separate C_6H_{12} and C_6D_{12} isotopic experiments, KIE values for step (1) in Scheme 1 (2.5 at 403 K from above) reflect

the cleavage of O–H or O–D bonds in H^* and D^*, respectively, when using R_HOOH or R_DOOD reactants. The activation of ROOH involves only the cleavage of O–O bonds in ROOH; thus, only small secondary H/D isotope effects (<1.5, most typically 1.1–1.2) [39] are expected for reactions of R_HOOH and R_DOOD species. As a result, we lump $[R_HOOH]$ and $[R_DOOD]$ as one chemical species in the kinetic treatment that follows,

$$[R_HOOH] + [R_DOOD] = [ROOH]_{total} \tag{19}$$

to give a total ROOH decomposition rate,

$$r_{ROOH,total} = \left(k_{1,H}[H^*] + k_{1,D}[D^*]\right)[ROOH]_{total}. \tag{20}$$

In analogy with the ROOH decomposition rates in C_6H_{12} oxidation [Eq. (A.7) in Appendix A], measured ROOH decomposition rate constants for mixed C_6H_{12}–C_6D_{12} reactants ($k_{1,mixed}$) correspond to the slope of the (alcohol + ketone) formation rate versus $[ROOH]_{total}$ divided by 3,

$$\begin{aligned} r_{(ROH+R(-H)=O)total} &= 3k_{1,mixed}[ROOH]_{total}[L] \\ &= k_{exp,mixed}[ROOH]_{total}[L]. \end{aligned} \tag{21}$$

Combining Eqs. (20) and (21) gives an equation relating ROOH decomposition rate constants in separate and mixed reactant measurements,

$$\left(k_{1,H}[H^*] + k_{1,D}[D^*]\right) = k_{1,mixed}[L], \tag{22}$$

in which $[H^*]$ and $[D^*]$ concentrations reflect (as shown below) the KIEs for the step in which H^* and D^* form [step (5)].

To obtain KIE values for C–H bond activation steps from product measurements, we need to consider the steps in which various R groups enter and exit the catalytic cycles. For instance, ROH forms in step (2) from ROOH molecules reacting in step (1) and from RH reacting in step (5). R(–H)=O from step (4) and ROOH from step (6) form using RH molecules that reacted in steps (2) and (6) (via R^* and ROO^* intermediates). The pseudo-steady-state assumption for H^* and D^* requires that steps (1) and (5) proceed at equal rates,

$$r_5 = r_{5,RH} + r_{5,RD} = k_{1,mixed}[ROOH]_{total}[L] \tag{23}$$

and the relative amounts of RH and RD reacting in step (5) are then determined by the KIE for this step (KIE_5),

$$r_{5,RH} = \left[\frac{KIE_5}{1 + KIE_5}\right] k_{1,mixed}[ROOH]_{total}[L] \tag{24}$$

and

$$r_{5,RD} = \left[\frac{1}{1 + KIE_5}\right] k_{1,mixed}[ROOH]_{total}[L]. \tag{25}$$

The total rate of R_DOD formation is the combined rate of R_DOOD decomposition in step (1) and of RD reactions in step (5),

$$\begin{aligned} r_{R_DOD} &= k_{1,mixed}[R_DOOD][L] \\ &\quad + \left[\frac{1}{1 + KIE_5}\right] k_{1,mixed}[ROOH]_{total}[L], \end{aligned} \tag{26}$$

which can be rearranged to give a KIE_5 value of

$$KIE_5 = \frac{k_{1,mixed}[ROOH]_{total}[L]}{r_{R_DOD} - k_{1,mixed}[R_DOOD][L]} - 1. \tag{27}$$

All of the terms in Eq. (27) can be measured independently from our experiments. Mixed C_6D_{12}–C_6H_{12} reactants gave a $k_{exp,mixed}$ ($3k_{1,mixed}$) value of 0.34 [mol ROH + R(–H)=O] (mol Mn_{redox})$^{-1}$ h^{-1}, leading to a KIE_5 value of 2.9 ± 0.5 from Eq. (27).

KIEs for step (5) also determine the rates at which H^* and D^* form; as a result, the rates for step (1) for mixed and separate C_6D_{12}–C_6H_{12} reactants can be used to confirm the KIE_5 estimates given above. Steady-state H^* and D^* surface coverages reflect their respective formation and consumption rates; thus, H^*, which forms 2.9 times faster than D^*, must also react 2.9 times faster than D^* at steady state. The ratio of the total H^* and D^* consumption rates (2.9) and the previously obtained KIE_1 value of 2.5 for their relative reactivity give a $[H^*]/[D^*]$ ratio of 1.16 (2.9/2.5) during oxidation of equimolar C_6H_{12}–C_6D_{12} mixtures. For sites predominantly present as H^* and D^* [Eq. (17)], the fractional $[H^*]$ surface coverage,

$$\Theta_H = \frac{[H^*]}{[L]}, \tag{28}$$

is then 0.54, and the rest of the surface is covered with D^*. These surface coverages can be used to estimate the ratio of first-order rate constants for ROOH decomposition in separate and mixed C_6H_{12}–C_6D_{12} oxidation experiments by rearranging Eq. (22) to give

$$\frac{k_{1,mixed}}{k_{1,H}} = \frac{k_{1,H}[H^*] + k_{1,D}[D^*]}{k_{1,H}[L]} = \Theta_H + \frac{1}{KIE_1}\Theta_D, \tag{29}$$

and inserting the measured values of Θ_H (0.54) and KIE_1 (2.5). This approach leads to a $k_{1,mixed}/k_{1,H}$ value of 0.72. We can also estimate $k_{1,mixed}/k_{1,H}$ independently from ROOH decomposition rate constants with mixed C_6H_{12}–C_6D_{12} ($k_{exp,mixed} = 3k_{1,mixed} = 0.34$) and separate C_6H_{12} ($k_{exp} = 3k_{1,H} = 0.46$) oxidation experiments, which give a $k_{1,mixed}/k_{1,H}$ value of 0.74. Thus, the two independent methods give essentially identical $k_{1,mixed}/k_{1,H}$ values, confirming the consistency of the Θ_H, KIE_1 and KIE_5 values obtained in mixed and separate experiments. This is an important conclusion, because hydroperoxide concentrations differ between these two types of experiments, and the agreement confirms both the broad validity of the mechanistic conclusions and the accurate accounting for $[R_HOOH]$ and $[R_DOOD]$ species in the interpretation of mixed C_6H_{12}–C_6D_{12} oxidation measurements. The confirmation of the ROOH decomposition kinetics and of the negligible contributions of isotopic mixing between C_6H_{12} and C_6D_{12} to KIE values in mixed experiments lead us to now consider the pathways and isotopic effects for the steps responsible for ROOH formation.

Reactions of mixed C_6H_{12}–C_6D_{12} reactants can probe the nature of ROOH formation steps, in addition to the overall RH oxidation (Figs. 11b and 11c), which involves RH activation steps that do not proceed through ROOH intermediates such as step (5) in Scheme 1, in which ROH forms directly from RH.

The total ROOH formation rate ($r_{ROOH,form}$) is the sum of the net rate of ROOH appearance in products ($r_{ROOH,net}$) and the rate of ROOH consumption in step (1),

$$r_{ROOH,form} = r_{ROOH,net} + r_{ROOH,dec} = r_{ROOH,net} + k_1[ROOH][L]. \quad (30)$$

The ratio of the total formation rates of R_HOOH and R_DOOD then gives a KIE value of 6.8 ± 0.5 for the total ROOH formation rate in mixed reactant experiments for all reaction times after the induction period. During the induction period, direct activation of RH by Mn^{3+} sites in step (12) also contributes to ROOH formation. The KIE value obtained for total ROOH formation rates is larger than for RH reactions with OH^* [2.9 for step (5)], indicating that the extent of C–H bond breaking to form the corresponding transition state is greater for H abstraction from RH with ROO^* in step (6) than for direct RH oxidation to ROH by more reactive OH^* species involved in step (5), consistent with a more exothermic nature and lower activation energy of the latter process.

Small normal KIEs (<2) have been thought to reflect the radical nature of H-abstraction pathways, whereas larger values are ascribed instead to activation pathways involving metal–oxo intermediates [40]. Yet KIE values for C–H bond activation for radical and metal–oxo pathways depend sensitively on the identity of the abstracting species and the strength of the relevant C–H bond, because more endothermic steps depend more strongly on C–H bond energies and give higher KIE values for a given hydrogen abstractor. For instance, *tert*-butoxy radicals abstract H from methyl groups in dimethylanilines and arylalkanes with KIE values of 1.5 for weak C–H bonds, but with much larger KIE values (∼6) for stronger C–H bonds, even though *tert*-butoxy abstraction pathways are identical in all of these processes [41]. Interestingly, a very similar range of KIE values (1.5–6) was obtained for activation of the same set of C–H bonds by a metal–oxo complex in cytochrome P450 [41]. A broad range of KIE values was also measured for H abstraction from alkanes on various Mn and Fe metal–oxo species [42,43]. Similarly to H abstraction by metal–oxo species, the reactivity of an abstracting radical determines KIE values for the activation of a given C–H bond. More reactive radicals (e.g., OH and Cl) give smaller KIE values than less reactive ones (e.g., Br and ROO) [36]. H_2O_2 molecules, which form highly active OH radicals as intermediates, give low KIE values (1–2) in alkane oxidation reactions [40,44], whereas KIE values with O_2 as the oxidant are much larger, because O_2 forms different radical-like intermediates than H_2O_2. In fact, the overlapping KIE values for radical and metal–oxo pathways make the use of KIE values to distinguish among various routes equivocal in the absence of the mechanistic analysis that we provide here.

At this point, we consider the origin of the large overall KIE values (∼60) measured for total cyclohexane oxidation rates on MnAPO-5 at 403 K. KIE values are larger for ROOH formation (6.8 ± 0.5) than for ROOH decomposition (2.5 ± 0.5). These differences lead to higher $k_{decomposition}/k_{formation}$ ratios for R_DOOD than for R_HOOH, which lead in turn to much lower concentrations of [R_DOOD] than [R_HOOH] at each reaction time. These lower [R_DOOD] values, the first-order nature of hydroperoxide decomposition to products, and the KIE values for this decomposition step combine to give the very high KIE values measured for the overall reaction. These high values merely reflect a sequence of elementary steps each with a normal KIE value, instead of any contributions from tunneling processes, often invoked to explain such high KIE values for many related reactions [40,45]. High KIE values must be considered in the context of the details of the sequence of elementary steps involved [46], not as a direct reflection of any one elementary step, unless confirmed by rigorous independent kinetic measurements and analyses. The mechanistic complexity of typical oxidation pathways, whether proceeding via bound or radical intermediates, requires that we also detect primary products involved in subsequent reactions and the corresponding isotope effects for the formation of such intermediates. This study provides a specific example of the essential nature of this approach, as well as specific evidence for a sequence of elementary steps involving bound versions of reactive intermediates typically considered to exist instead as radical species even when specific inorganic catalytic sites are present and heterogeneous activation steps are invoked.

The catalytic sequence proposed here and supported by kinetic and isotopic evidence involves kinetically relevant ROOH decomposition on divalent Mn sites. These conclusions are consistent with the first-order dependence of ROH + R(–H)=O formation rates on [ROOH] and with the prevalence of Mn^{2+} as the most abundant reactive intermediate, detected by UV–visible spectroscopy and by qualitative visual inspection of color. C–H bond activation to form ROOH proceeds primarily via abstraction of H atoms from RH using of ROO^* species, but also by $^tBuOO^*$ species when TBHP is present as an initiator and by Mn^{3+} during initial stages of reaction on samples treated in O_2 before reaction. This sequence of elementary steps (Scheme 1) is inconsistent with the direct docking of RH species onto trivalent sites, which was invoked to explain selective terminal oxidation of linear alkanes [19]. ROOH formation and ROOH decomposition pathways in Scheme 1 are essential requirements for the correct interpretation of reactant and transition-state shape-selectivity in alkane oxidation on well-characterized MnAPO-18 and MnAPO-5 materials [32] and on Mn-exchanged zeolitic materials [47], as we report separately. Specifically, accurate measurements of ROOH intermediates and a rigorous assessment of their role in complex propagation and termination cycles on surfaces are required before any unequivocal connections can be established between shape-selectivity effects and specific elementary steps and before any sensible guidance can be provided for the design of channels or active sites for positional or reactant selectivity in these catalytic systems.

4. Conclusion

Combined rates of ROH + R(–H)=O synthesis during RH oxidation on MnAPO-5 are first order in [ROOH] and proportional to the number of redox-active Mn sites. Together with UV–visible evidence for Mn^{2+} as the MASI during steady-state cyclohexane oxidation, the first-order ROOH dependence

indicates that ROOH decomposition on Mn^{2+} is a kinetically relevant step. A proposed catalytic cycle for ROOH decomposition and ROOH formation proceeding via adsorbed intermediates accounts for measured ROH/R(–H)=O product ratios of close to 2. The KIE for ROOH decomposition in the region of overlapping R_HOOH and R_DOOD concentrations is 2.5 at 403 K, consistent with cleavage of the O–H(D) bond in the Mn^{2+}–O–H(D) sites in this elementary step. Mn^{3+} species, initially present in air-treated MnAPO-5, activate C–H bonds at early stages of the reaction and lead to shorter initial induction periods required for ROOH-mediated pathways, but do not play a significant role beyond the induction period. Instead, ROOH formation occurs predominantly through activation of C–H bonds in RH by ROO^* species in a step that gives a KIE value of 6.8. RH activation by OH^* species in the ROOH decomposition cycle gives a lower KIE value of 2.9, consistent with the more exothermic nature of RH reacting with OH^* than with ROO^*. Addition of TBHP led to higher ROOH synthesis rates via H abstraction from RH by $^tBuOO^*$ species, but without influencing ROOH decomposition rate constants, suggesting that the presence of TBHP does not influence ROOH decomposition pathways. Because of the intermediate nature of ROOH in RH oxidation with O_2, the approach outlined here of measuring catalytic ROOH formation and ROOH decomposition rates as function of [ROOH] was essential for obtaining rate constants and KIE values for the kinetically relevant elementary steps involved in Mn-catalyzed cyclohexane oxidation.

Acknowledgments

These studies were supported by a research grant from ExxonMobil Research and Engineering Co.

Appendix A. Derivation of rate expressions

The kinetically relevant step for ROOH decomposition is step (1) in Scheme 1, where ROOH reacts with H^*; the rate of this step is given by

$$r_{ROOH} = k_1[ROOH][H^*], \tag{A.1}$$

where rate constants k_i are used for elementary steps (i) in Scheme 1. To solve for $[H^*]$, we solve the dynamic mole balances of all surface intermediates in Scheme 1 (H^*, RO^*, R^*, ROO^*, and OH^*), and apply the pseudo-steady-state assumption for these species to obtain all species in terms of $[H^*]$. The site balance over the total number of sites, [L], is given by the sum of all intermediates,

$$[L] = [H^*] + [RO^*] + [R^*] + [ROO^*] + [OH^*], \tag{A.2}$$

which all can be expressed in terms of their dependence on $[H^*]$,

$$[L] = [H^*] + \frac{k_1[H^*][ROOH]}{k_2[RH]} + \frac{k_4 + k_6[RH]}{k_3[O_2]}\frac{k_1[H^*][ROOH]}{k_4} + \frac{k_1[H^*][ROOH]}{k_4} + \frac{k_1[H^*][ROOH]}{k_5[RH]}. \tag{A.3}$$

From Eq. (A.3), we can solve for $[H^*]$ in terms of measurable quantities such as [ROOH], [RH], and $[O_2]$ as well as the total active site concentration [L],

$$[H^*] = [L]\left[1 + k_1[ROOH]\left(\frac{1}{k_2[RH]} + \frac{k_4 + k_6[RH]}{k_3k_4[O_2]} + \frac{1}{k_4} + \frac{1}{k_5[RH]}\right)\right]^{-1}, \tag{A.4}$$

which can be inserted into the expression for the kinetically relevant step [Eq. (A.1)] to get the total rate,

$$r_{ROOH} = k_1[ROOH][H^*] = k_1[ROOH][L]\left[1 + k_1[ROOH]\left(\frac{1}{k_2[RH]} + \frac{k_4 + k_6[RH]}{k_3k_4[O_2]} + \frac{1}{k_4} + \frac{1}{k_5[RH]}\right)\right]^{-1}, \tag{A.5}$$

in terms of measurable quantities. With $[H^*]$ as the MASI as predicted by the first-order rate dependence on [ROOH] (i.e., $[H^*] = [L]$), all denominator terms except for unity vanish, and we obtain

$$r_{ROOH} = k_1[ROOH][H^*] = k_1[ROOH][L]. \tag{A.6}$$

From the catalytic cycle starting with the reaction of ROOH with $[H^*]$, two RHs also react, giving a total rate of three alkane-derived products [2 ROH and R(–H)=O] per cycle,

$$r_{ROH+R(-H)=O} = k_{exp}[ROOH][L] = 3k_1[ROOH][L], \tag{A.7}$$

where k_{exp} is the experimentally determined first-order rate constant.

References

[1] R.A. Sheldon, J.K. Kochi, Metal-Catalyzed Oxidations of Organic Compounds, Academic Press, New York, 1981.
[2] C.L. Hill, Activation and Functionalization of Alkanes, Wiley, New York, 1989.
[3] U. Schuchardt, D. Cardoso, R. Sercheli, R. Pereira, R.S. de Cruz, M.C. Guerreiro, D. Mandelli, E.V. Spinace, E.L. Fires, Appl. Catal. A: Gen. 211 (2001) 1.
[4] C. Batiot, B.K. Hodnett, Appl. Catal. A: Gen. 137 (1996) 179.
[5] J.A. Labinger, J. Mol. Catal. A: Chem. 220 (2004) 27.
[6] S.T. Wilson, B. Lok, E.M. Flanigen, U.S. Patent 4310440, 1982.
[7] S.T. Wilson, E.M. Flanigen, U.S. Patent 4567029, 1986.
[8] B.M. Weckhuysen, R.R. Rao, J.A. Martens, R.A. Schoonheydt, Eur. J. Inorg. Chem. (1999) 565.
[9] M. Hartmann, L. Kevan, Chem. Rev. 99 (1999) 635.
[10] M. Hartmann, L. Kevan, Res. Chem. Intermed. 28 (2002) 625.
[11] S.S. Lin, H.S. Weng, Appl. Catal. A: Gen. 105 (1993) 289.
[12] S.S. Lin, H.S. Weng, Appl. Catal. A: Gen. 118 (1994) 21.
[13] D.L. Vanoppen, D.E. Devos, M.J. Genet, P.G. Rouxhet, P.A. Jacobs, Angew. Chem. Int. Ed. Engl. 34 (1995) 560.
[14] D.L. Vanoppen, P.A. Jacobs, Catal. Today 49 (1999) 177.
[15] P. Concepcion, A. Corma, J.M. Lopez Nieto, J. Perez-Pariente, Appl. Catal. A: Gen. 143 (1996) 17.
[16] I. Belkhir, A. Germain, F. Fajula, E. Fache, J. Chem. Soc., Faraday Trans. 94 (1998) 1761.
[17] G. Sankar, R. Raja, J.M. Thomas, Catal. Lett. 55 (1998) 15.
[18] R. Raja, J.M. Thomas, Chem. Commun. (1998) 1841.
[19] J.M. Thomas, R. Raja, G. Sankar, R.G. Bell, Nature 398 (1999) 227.
[20] R. Raja, G. Sankar, J.M. Thomas, J. Am. Chem. Soc. 121 (1999) 11926.

[21] J.M. Thomas, R. Raja, G. Sankar, R.G. Bell, Stud. Surf. Sci. Catal. 130 (2000) 887.
[22] A.F. Masters, J.K. Beattie, A.L. Roa, Catal. Lett. 75 (2001) 159.
[23] Z. Hou, B. Han, L. Gao, Z. Liu, G. Yang, Green Chem. 4 (2002) 426.
[24] P. Tian, L. Xu, T. Huang, P. Xie, Z.M. Liu, Chem. J. Chin. Univ. 23 (2002) 656.
[25] P. Tian, Z. Liu, Z. Wu, L. Xu, Y. He, Catal. Today 93 (2004) 735.
[26] J.D. Chen, R.A. Sheldon, J. Catal. 153 (1995) 1.
[27] Y. Kamiya, K.U. Ingold, Can. J. Chem. 42 (1964) 2424.
[28] J.F. Black, J. Am. Chem. Soc. 100 (1978) 527.
[29] F.A. Chavez, J.M. Rowland, M.M. Olmstead, P.K. Mascharak, J. Am. Chem. Soc. 120 (1998) 9015.
[30] F.A. Chavez, P.K. Mascharak, Acc. Chem. Res. 33 (2000) 539.
[31] B. Moden, L. Oliviero, J. Dakka, J.G. Santiesteban, E. Iglesia, J. Phys. Chem. B 108 (2004) 5552.
[32] B. Moden, B.-Z. Zhan, J. Dakka, J.G. Santiesteban, E. Iglesia, in preparation.
[33] J.D. Chen, J. Dakka, R.A. Sheldon, Appl. Catal. A: Gen. 108 (1994) L1.
[34] R.A. Sheldon, M. Wallau, I.C.W.E. Arends, U. Schuchardt, Acc. Chem. Res. 31 (1998) 485.
[35] I.C.W.E. Arends, R.A. Sheldon, Appl. Catal. A: Gen. 212 (2001) 175.
[36] G.A. Russell, J. Am. Chem. Soc. 78 (1957) 3871.
[37] E.T. Denisov, T.G. Denisova, Handbook of Antioxidants, second ed., CRC Press, Boca Raton, 2000.
[38] L. Melander, J.M. Sanders, Reaction Rates of Isotopic Molecules, Wiley, New York, 1980.
[39] T.H. Lowry, K.S. Richardson, Mechanism and Theory in Organic Chemistry, Haper and Row, New York, 1987.
[40] A.M. Khenkin, A.E. Shilov, New J. Chem. 13 (1989) 659.
[41] J.I. Manchester, J.P. Dinnocenzo, L. Higgins, J.P. Jones, J. Am. Chem. Soc. 119 (1997) 5069.
[42] B. Meunier, Chem. Rev. 92 (1992) 1411.
[43] A. Sorokin, A. Robert, B. Meunier, J. Am. Chem. Soc. 115 (1993) 7293.
[44] E.S. Rudakov, L.K. Volkova, V.P. Tretyakov, React. Kinet. Catal. Lett. 16 (1981) 333.
[45] M.H. Glickman, J.S. Wiseman, J.P. Klinman, J. Am. Chem. Soc. 116 (1994) 793.
[46] A. Thibblin, P. Ahlberg, Chem. Soc. Rev. 18 (1989) 209.
[47] B.-Z. Zhan, B. Moden, J. Dakka, J.G. Santiesteban, E. Iglesia, in preparation.